POAC'23
Glasgow, United Kingdom

Proceedings of the 27th International Conference on
Port and Ocean Engineering under Arctic Conditions
12-16 June 2023, Glasgow, United Kingdom

Meso-scale stress relaxation test on floating sea ice

Aleksey Marchenko[1], Evgeny Karulin[2,3], Peter Chistyakov[4],
Marina Karulina[3], Alexander Sakharov[4]
[1] The University Centre in Svalbard, Longyearbyen, Norway
[2] State Marine Technical University, St.-Petersburg, Russia
[3]Krylov State Research Centre, St.-Petersburg, Russia
[4]Lomonosov Moscow State University, Moscow, Russia

ABSTRACT

Meso-scale stress relaxation test was performed with hydraulic indentation rig equipped with two vertical plates applying load in the horizontal direction to the ice edges over entire thickness of the ice. The indentation rig was placed in a pool cut in floating sea ice, and two hydraulic cylinders applied horizontal load 120 kN to the ice edges in the pool over entire ice thickness by two vertical metal plates 60x80 cm. The load was applied to the ice during 10 min and then removed. The ice compression in longitudinal to the loading and transversal directions was recorded with 4 pressure cells Geokon with diameter 10 cm. The cells were frozen in sea ice in the front of the indentation plate on the depth 20 cm from the ice surface. Pressure cells recorded increasing pressure during the loading time and relaxation of stresses after the unloading. Numerical simulations of the test were performed in FE software Comsol MultiPhysics where sea ice was modeled by viscoelastic Burgers material. Rheological constants of the model were determined in the laboratory tests with ice cores taken from the location of the field test. Details of the field measurements and results of numerical simulations are discussed in the paper.

KEY WORDS: Sea Ice; Viscoelastic Rheology; Meso-Scale Test; Numerical Simulations.

1. INTRODUCTION

It is known that polycrystalline ice has elastic, viscous and anelastic properties (Cole, 2020). Columnar sea ice demonstrates anisotropy of stress relaxation and elastic lag in vertical and horizontal directions (Marchenko et al., 2021). Influence of sea ice compression on

permeability was discovered in meso-scale tests (Renshaw et al., 2018). Influence of liquid brine on thermal deformations and stresses in sea ice was discussed in several paper (Malmgrem, 1927; Cox, 1983; Johnson and Metzner, 1990; Levis, 1998; Marchenko and Lishman, 2017; Marchenko, 2018). Influence of porous fluid on mechanical deformations and stresses of solids was investigated in different materials (Nikolaevskiy, 1996; Chen et al., 2021) but was not discussed previously for the application to sea ice problems.

Rheological properties of polycrystalline ice are characterized by elasticity, stress relaxation, creep, and elastic lag. Burgers material is simplest model describing this set of rheological properties of materials (Ashton, 1986). Rheological constants of the Burgers model characterizing viscous and anelastic properties of materials can be determined from tests on stress relaxation and loading-unloading tests (Marchenko et al., 2021). Leak of brine from the ice due to sea ice permeability influences test results in the laboratory experiments. In the present paper we describe meso-scale loading-unloading test performed on floating sea ice in March 2018, formulate main results of the test, and compare it with the results of numerical simulations of the test performed with Burgers material model of ice.

2. FIELD WORK

The field works were organized on land fast ice in the Vallunden lagoon near Svea in the Van-Mijen Fjord, Spitsbergen, in March 2018 (Fig. 1a). Sea water salinity in the lagoon is the same as in the fjord, and sea ice in the lagoon is similar sea ice in the fjord. The ice thickness was 60 cm in the beginning of the field works on March 5. The ice was covered by thin layer of snow (Fig. 1b). Two tents were installed on sea ice to store equipment and to investigate thin sections of ice in polarized light by Rigsby Stage. Figure 2a shows vertical slab of sea ice with dimensions 60x60 cm. Top layer of ice of 20 cm thickness had granular structure with grain size of 1-3 mm. The ice had columnar structure S2 below the top layer with grain diameters slightly below 1 cm. Lateral surface of columns had not polygonal structure with many small irregularities which is typical for that place (Marchenko et al., 2020). The mean salinity of sea ice was 6 ppt. Ice temperature changed from -15 C at the ice surface to the freezing point -1.9 C near the ice bottom.

a) 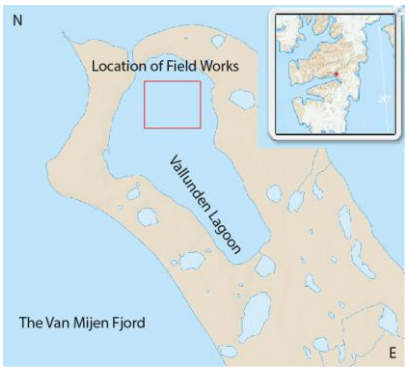

b) 

Figure 1. (a) Location of field works. (b) Organizing of field works on sea ice.

Schematic of the test is shown in Fig. 3, and photographs of the test are shown in Fig. 4. The indentation rig equipped with two hydraulic cylinders and two metal plates P1,2 (60x80 cm) mounted on the cylinders was submerged into the pool (120x87cm) made in sea ice. Hydraulic cylinders HCA and HCB are shown in Fig. 3. In the working position HCA was near the water surface in the pool, and HCB was submerged (Fig. 4). When the cylinders are powered by the hydraulic station their pistons start to move in the horizontal direction and transfer their motion to the plates P1 and P2. Since the plates are in contact with the ice edges

in the pool their motion creates horizontal loads on the ice edges. The width of ice edges was 87 cm, and the width of plates P1 and P2 was 60 cm. The principle of indenter work and characteristics of the equipment are described in (Marchenko e al., 2019). Above the ice the indentation rig is hanged by chains on A shape metal frame on sledges. Pistons of the hydraulic cylinders are moved by oil pressure pumped by the hydraulic station taking electric power from generator. Maximal power of each hydraulic cylinder is 30 t.

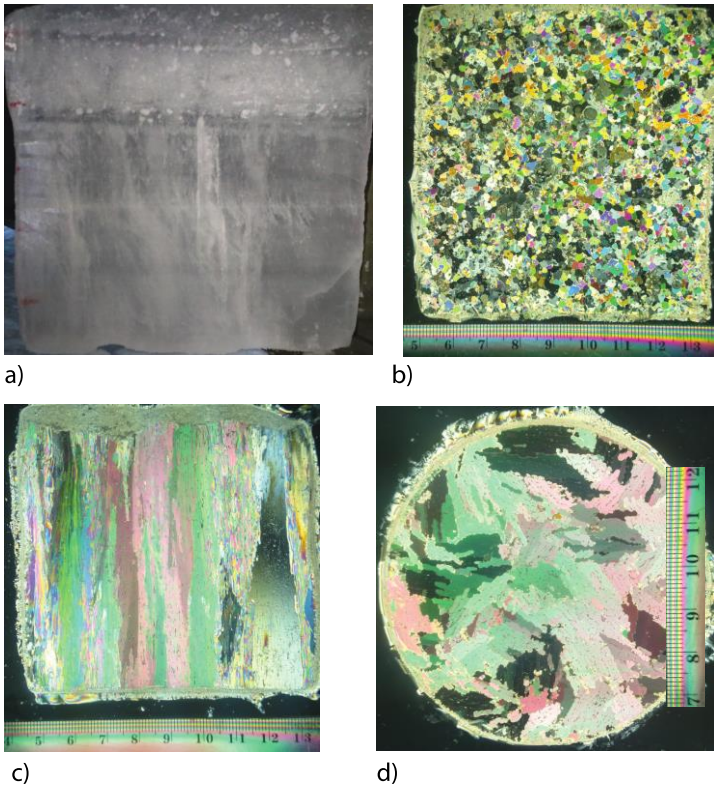

Figure 2. Photographs of sea ice slab (a). Thin sections of granular sea ice from top layer (b). Vertical (c) and horizontal (d) thin sections of columnar ice below the top layer. (Photographs are provided by Dave Cole)

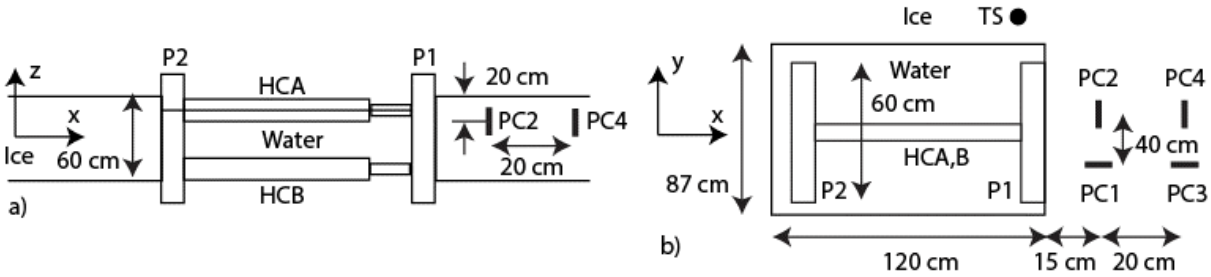

Figure 3. Schematic of meso-scale test on stress relaxation in the vertical (a) and horizontal (b) planes.

Four pressure cells Geokon (PC1-PC4) were frozen into the ice on 20 cm depth in the front of indentation plate P1 (Fig. 3). Diameter of each pressure cell is 10 cm. Two pressure cells PC1 and PC3 measured ice pressure in the transversal direction to the motion of plates P1 and P2. Another two pressure cells PC2 and PC4 measured ice pressure in parallel direction to the force applied by the cylinders to the ice edges in the pool. Black cylinders in Fig. 4 are the rubber cover of the power cables of the pressure cells.

Figure 4. Photographs of the indentation rig during the test.

In the test constant load of 120 kN was applied to the ice edges over entire ice thickness 60 cm during 10 min and then released. The load and stroke of each cylinder were recorded by the load and stroke sensors mounted inside the cylinders. Sampling interval of the sensors was set to 0.02 s. Synchronously the ice pressure was recorded by pressure cells PC1-PC4. Sampling interval of the pressure cells was set to 10 s.

The ice temperature was measured versus time by temperature string Geoprecision with spatial resolution 5 cm. The temperature string location is marked TS in Fig. 3b. The temperature string is also visible in Fig. 4. Cores of natural sea ice and sea ice compressed in the front of the plate P1 were drilled out after the test to measure the ice temperature and salinity.

3. RESULTS

Blue and yellow lines in Fig. 5a show the forces in the cylinders HCA and HCB. The force in HCA was much large the force in HCB. In Figure 5b stroke sensor of HCA shows 5 mm displacement during the test from t=200 s to t=760 s. The stroke of HCB didn't change during this time. Total force of about 120 kN influences nominal pressure on the ice distributed over the contact surface of the plate P1 with the ice edge (60x60 cm). Blue line in Fig. 6a shows the nominal pressure versus time. The nominal pressure was about 300 kPa during the stage of active loading from t=200 s to t=760 s. Colored lines show the ice pressures recorded by the cells P1-P4 on the loading stage of the test. One can see that PC2 and PC4 measuring ice pressure along the direction of applied load show almost similar pressures. PC1 recorded lower pressure, and pressures measured by PC3 are much lower the other pressures. Pressure cells PC1, PC2 and PC4 show four events on pressure increase which are not visible in the forces applied by HCA and HCB. Time interval between the events of pressure increase was about 100 s.

Figure 6b shows ice pressures PC1-PC4 at the stage when the load on the ice edge in the pool was released. Pressure cells PC2 and PC4 demonstrate synchronous relaxation of ice pressure in time along the x-direction. Pressures recorded by the cells PC1 and PC3are much more stable, and to the end of the test by t=1400 s pressure PC1 is much larger the other pressures.

Figure 7 shows vertical profiles of ice temperature and salinity before (blue lines) and after (yellow lines) the test. Yellow lines correspond the temperature and the salinity of ice core taken from the compression zone in the front of the plate P1 after the test. One can see that ice temperature in the upper half of the ice sheet in compression zone increased after the test,

and ice salinity in compression zone decreased after the test. The temperature increase indicates the influence of water on the ice temperature. The decrease of ice salinity indicates a migration of liquid brine from the compression zone.

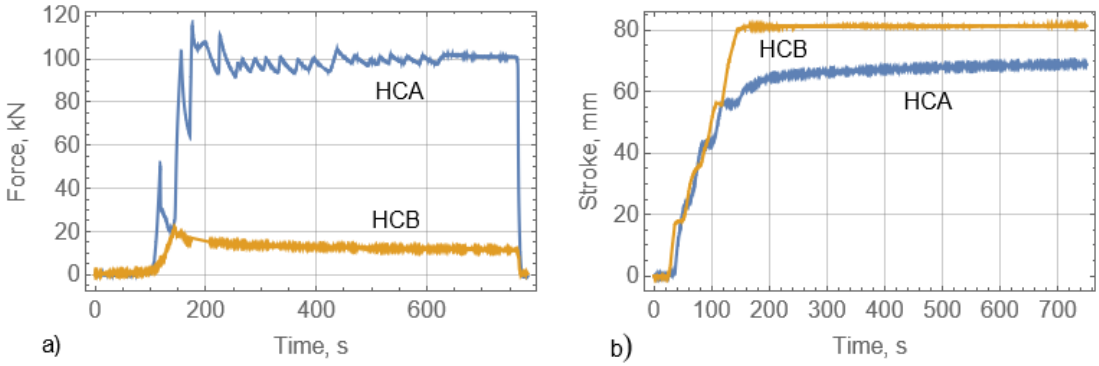

Figure 5. Forces (a) and strokes (b) versus time recorded by the load cells and stroke sensors installed in hydralic cylinders HCA and HCB.

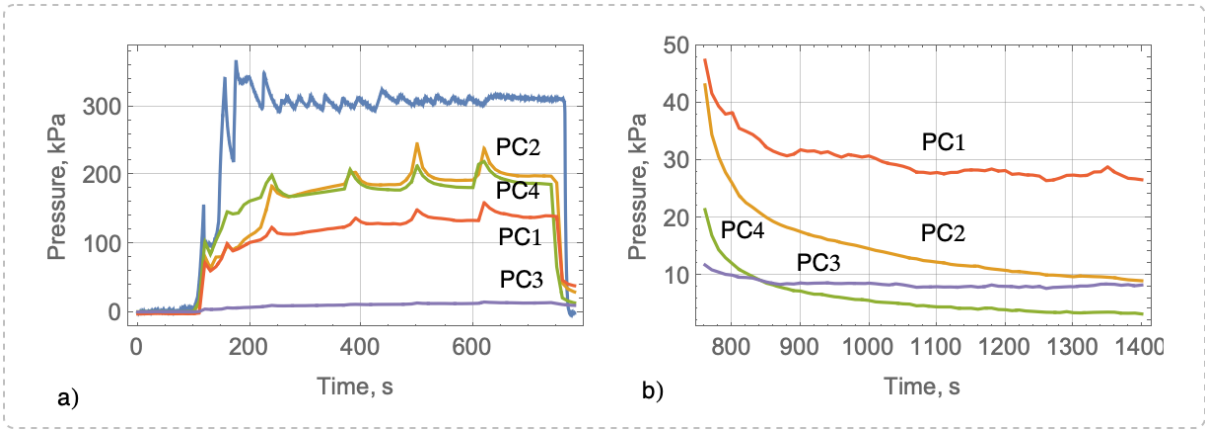

Figure 6. (a) Nominal pressure applied by the rig to the ice (blue line) and pressures measured by the pressure cells PC1-PC4 on the loading stage of the test versus time. (b) Pressures measured by the pressure cells PC1-PC4 versus time after the load was released.

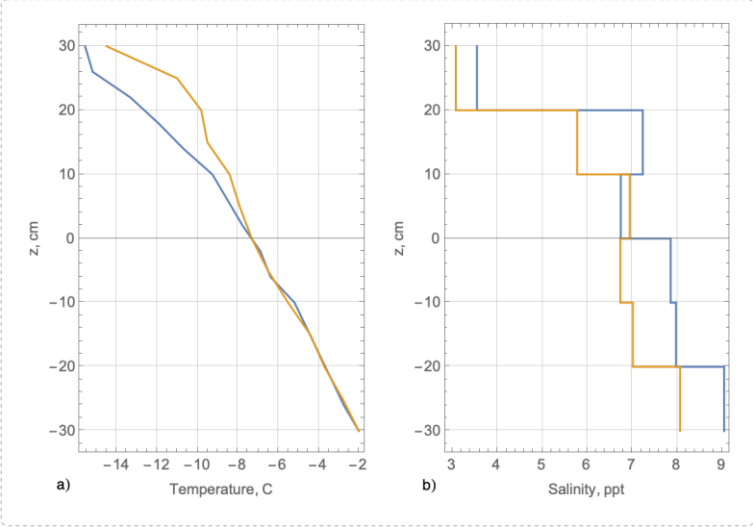

Figure 7. Ice temperature (a) and salinity (b) profiles before (blue lines) and after (yellow lines) test.

4. NUMERICAL SIMULATIONS

Figure 8 shows computational domain 10x10 m with thickness 0.6 m simulating sea ice. There is a rectangular cut 1.2x0.87 m in the middle of the domain simulating the pool for the indentation rig. Numerical simulations were performed by finite element software Comsol Multiphysics 5.4 using Structural Mechanics/Solid Mechanics/Heat Transfer/Multiphysics module with time dependent 3D solver. Heat Transfer module was used to simulate thermal stresses in the ice caused by sea water at the freezing point -1.9 C in the pool.

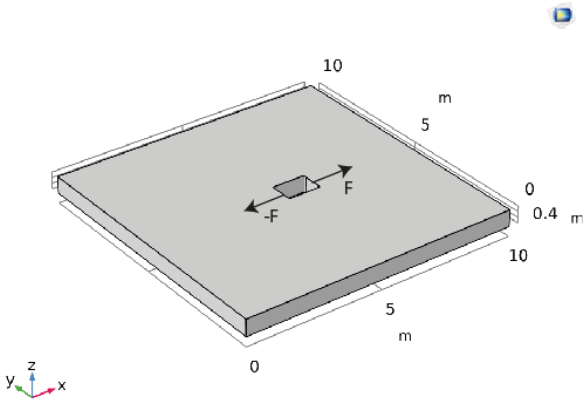

Figure 8. Computational domain.

Burgers material is used to simulate deformations of ice. Rheological equations of Burgers material are written in the deviatoric form

$$\sigma_{ii}=3K_M(\varepsilon_{ii}-\alpha\Delta T),\ e=\varepsilon', \qquad (1)$$

$$G_V\,\mathrm{dev}(e)+\eta_V\,\mathrm{dev}(e')=\eta_V\,G_V^{-1}\mathrm{dev}(\sigma'')+(\eta_V\eta_M^{-1}+G_V\,G_M^{-1})\,\mathrm{dev}(\sigma')+G_V\eta_M^{-1}\,\mathrm{dev}(\sigma)$$

where σ, ε, and e are stress, strain and strain rate tensors, T is temperature, K_M is volumetric elastic modulus, α is the linear coefficient of thermal expansion, G_M and G_V are elastic shear modulus of Maxwell and Voigt units, η_M and η_V are viscous shear coefficients of Maxwell and Voigt units. Constants K_M and G_M are expressed via the Young's modulus E_M and the Poisson's ratio ν_M by standard formulas following from the Hook's law. Rheological constants of Burgers material model are given in Table 1. In the Heat Transfer/Multiphysics module we used thermal conductivity 1.9 W/m·K, the heat capacity 3 kJ/kg·K.

In the initial time the linear temperature distribution with -2 C at the ice bottom and -15 C at the ice surface was set, and all stresses were set to zero. Temperature at the lateral surface of the cut in the middle of the computational domain changed from the linear distribution to -2 C during 100 s. Symmetry boundary conditions were used at the external lateral boundaries of the computational domain. Force F and force -F simulated actions of indentation plates P1 and P2 on the ice were applied in the opposite directions of the x-axis to the edges of the cut in the middle of the computational domain (Fig. 8). In the simulations the forces were given by the indentation pressures PI applied over an area 60x60 cm. The dependence of PI from time is shown in Fig. 9b by blue line. Free surface boundary conditions are used on the other

surfaces of the computational domain.

Table 1. Rheological constants of Burgers material model.

E_M, GPa	ν_M	G_V, GPa	η_M, GPa·s	η_V, GPa·s	ρ_i, kg/m^3	α, K^{-1}
2	0.3	1	60	60	920	$5 \cdot 10^{-5}$

Figure 9a shows simulated pressures PC1-PC4 with F=0, i.e. when the ice stresses are caused only by thermal action at the edges of the cut in the middle of the computational domain. Line colors corresponds to designations in Fig. 9b. Thermal stresses become small within 400 s. It means small influence of thermal stresses during active loading of sea ice in the field test. Simulations with active force F were started at the initial time t=-100 s, while active loading started at t=200 s. Therefore, the thermal stresses were small during active stage of the loading from t=200 s to t=800 s. Lines PC1-PC4 in Fig. 9b shows simulated pressures PC1-PC4. The indentation pressure versus time is shown by blue line PI. Oscillations in the solution are probably caused by an instability of numerical simulations. Pressures PC2 and PC4 are similar during the active stage of the loading. It corresponds well to the line PC2 and PC4 in Fig. 6a. Pressure PC1 in Fig. 9b is lower than in Fig. 6a. After the release of the load simulated pressures PC1 and PC2 become negative, and pressures PC2 and PC4 tend to zero in Fig. 9b. Thus, simulated pressures are very different from the pressures recorded during the test after the load was released (Fig. 6b).

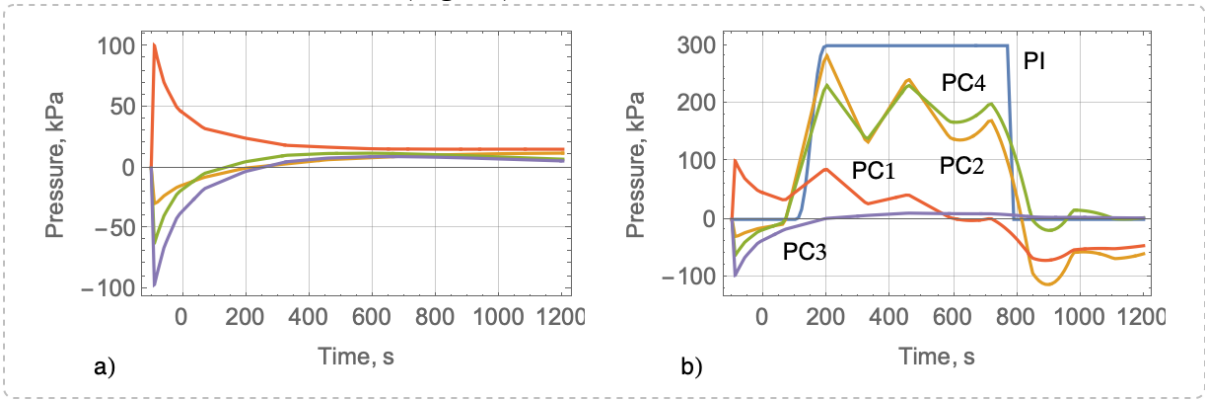

Figure 9. (a) Simulated dependencies of thermal pressure in ice in the points were pressure cells P1-P4 were deployed. (b) Simulated dependencies of ice pressures P1-P4 during the test. Nominal pressure applied to the ice during the test is shown by blue line.

5. CONCLUSIONS

Meso-scale test performed on floating sea ice demonstrated few effects which are not explained by viscoelastic properties of ice. It includes local rises and drops of ice pressure in compression zone which were most strong in the direction of compression, and different times of stress relaxation in the direction of compression and in the transversal direction after the load was removed. Local rises and drops of ice pressure were not related to the changes of oil pressure in hydraulic cylinders. The ice pressure was lower the nominal pressure of the loading plate P1 at the ice edge over the entire test. Decrease of ice salinity in compression zone indicated the migration of liquid brine from compression zone into the water and surrounding ice. Building up of porous pressure in liquid brine may influence ice structure, permeability, and stress relaxation processes in sea ice observed in the test. Drops of ice pressure during ice compression can be explained by events of brine migration through the

ice accompanied by changes of internal structure of ice. It also may explain slow rise of ice pressure in compression zone when nominal pressure at the ice edge varied around constant value of 300 kPa.

The work was supported by the Research Council of Norway through the IntPart project Arctic Offshore and Coastal Engineering in Changing Climate and SSG grant 311266. Authors thanks David Cole for the cooperation during the field works in Svea, March 2018.

REFERENCES

Ashton, G.,D., (Ed.), 1986. River and lake ice engineering. Water Resources Publications, Michigan, U.S.A.

Chen, X., Ti, F., Li, M., Liu, S., Lu, T., J., 2021. Theory of fluid saturated porous media with surface effects. J. of the Mechanics and Physics of Solids, 151, 104392.

Cole, D., M., 2020. On the physical basis for the creep of ice: the high temperature regime. *J. Glaciology*, 1-14.

Cox, G.,F.,N., 1983. Thermal expansion of saline ice. *J. Glaciology*. 29, 425–432.

Johnson., J.,B., Metzner, R.,C., 1990. Thermal expansion coefficients for sea ice. *J. Glaciology*., 36, 343–349.

Lewis, K.J., 1998. Thermomechanics of pack ice. *J. Geoph. Res*., 103, NC10, 21869-21882.

Malmgren F. 1927 On the properties of sea ice. In The Norwegian North Polar expedition with the “Maud” 1918–1925, Scientific results (ed. HU Sverdrup), vol. 1, no. 5, pp. 1–67. Bergen, Norway: Grieg.

Marchenko A, Lishman B., 2017. The influence of closed brine pockets and permeable brine channels on the thermo-elastic properties of saline ice. *Phil.Trans. R. Soc. A 375*: 20150351.

Marchenko, A., 2018. Thermo-mechanical loads of confined sea ice on structures. *Phil.Trans. R. Soc. A* 376: 20170341.

Marchenko, A., Karulin, E., Sakharov, A., Chistyakov, P., 2019. On the influence of the hydraulic characteristics of the rig during full-scale compression and indentation tests on sea ice. *Proceedings of POAC19,* 32.

Marchenko, A., et al., 2020. Influence of vibrations on indentation and compression strength of sea ice. *Proceedings of the IAHR International Symposium on Ice*.

Marchenko, A., Karulin, E., Chistyakov, P., 2021. Experimental investigation of viscous elastic properties of columnar sea ice. *Proceeding of POAC21,* 043.

Nikolaevskiy, V., N., 1996. Geomechanics and Fluidodynamics. Kluwer Academic Publishers, Dordrecht.

Renshaw, C. E., Marchenko, A., Schulson, E.M., Karulin, E., 2018. Effect of compressive loading on first-year sea-ice permeability. J. Glaciology, 64(245), 443-449.